

Optical Brewster Metasurfaces Exhibiting Ultrabroadband Reflectionless Absorption and Extreme Angular Asymmetry

Huiying Fan^{1,2}, Jensen Li,^{3,*} Yun Lai,^{4,†} and Jie Luo^{1,2,‡}

¹*School of Physical Science and Technology, Soochow University, Suzhou 215006, China*

²*Institute of Theoretical and Applied Physics, Soochow University, Suzhou, 215006, China*

³*Department of Physics, The Hong Kong University of Science and Technology, Clear Water Bay, Hong Kong, China*

⁴*National Laboratory of Solid State Microstructures, School of Physics, and Collaborative Innovation Center of Advanced Microstructures, Nanjing University, Nanjing 210093, China*



(Received 6 August 2021; accepted 1 October 2021; published 29 October 2021)

Impedance mismatch between free space and absorptive materials is a fundamental issue plaguing the pursuit of high-efficiency light absorption. In this work, we design and numerically demonstrate a type of nonresonant impedance-matched optical metasurface exhibiting ultrabroadband reflectionless absorption based on the anomalous Brewster effect, which is denoted as an optical Brewster metasurface here. Interestingly, the Brewster metasurface exhibits a type of extreme angular asymmetry: a transition between perfect transparency and perfect absorption appears when the sign of the incident angle is changed. Such a remarkable phenomenon originates from the coexistence of traditional and anomalous Brewster effects. Guidelines for material selection based on an effective-medium description and strategies such as the integration of a metal back-reflector or a folded metasurface are proposed to improve the absorption performance. Finally, a gradient optical Brewster metasurface exhibiting ultrabroadband and near-omnidirectional reflectionless absorption is demonstrated. Such high-efficiency asymmetric optical metasurfaces may find applications in optoelectrical and thermal devices like photodetectors, thermal emitters, and photovoltaics.

DOI: 10.1103/PhysRevApplied.16.044064

I. INTRODUCTION

Optical absorbers that exhibit ultrabroadband perfect absorption of light are promising for many applications, such as photodetectors [1], thermal emitters [2], and photovoltaics [3]. To achieve perfect absorption, the incident light should be completely absorbed without any reflection or transmission. The transmission of light can be easily eliminated by increasing the thickness of the absorptive materials to a scale much larger than the wavelength. On the contrary, the elimination of the reflection caused by impedance mismatch at the air-absorber interface is challenging to achieve in an ultrabroad spectrum. This is because the impedance of air is a fixed real value, while the impedance of absorptive materials is generally a frequency-dependent complex value, making impedance matching in an ultrabroad spectrum an extremely difficult task.

The traditional method to mitigate the difficulty of an ultrabroadband impedance mismatch is based on surface topography [4,5], like the absorbing wedges for microwaves, which can gradually vary the effective impedance from that of air to that of the absorptive material. However, at optical frequencies, the scale of such wedges is reduced to micrometers and nanometers [6], which makes fabrication more challenging. Another method is to introduce resonant structures to achieve destructive interference of the reflected light. Typical examples are the Dallenbach [7] and Salisbury [8] screens. Recent advances of plasmonics, metamaterials, and metasurfaces have provided efficient ways to manipulate light-matter interactions, making it possible to realize optically thin absorbers [9–18], but, due to the resonant nature, the absorption bandwidth is generally limited. To broaden the bandwidth, the complex engineering of dispersion [19,20], multiresonances at different wavelengths [21–29], and random plasmonic nanostructures [30–33] are usually required. In addition, angular-symmetric absorption is usually obtained, while the issue of absorption-related angular dependence or angular asymmetry was rarely investigated until very recently [34–37].

*jensenli@ust.hk

†laiyun@nju.edu.cn

‡luojie@suda.edu.cn

Notably, ultrabroadband zero reflection and angular dependence both inherently exist in optics; this is known as the Brewster effect (BE) [38,39]. For lossless dielectrics with almost constant permittivity, such as silica (SiO_2) and magnesium fluoride (MgF_2), zero reflection at the air-dielectric interface is easily achieved at the Brewster angle over a broad spectrum for transverse-magnetic (TM) polarization. However, if loss is introduced to the permittivity of dielectrics, a phase difference between the electric and magnetic fields will appear, thus leading to a mismatch between the fields in free space and dielectrics. In this scenario, reflection will appear, and the BE will be destroyed. Due to this dilemma, although the BE has an inherently ultrabroad bandwidth, it had not been applied for ultrabroadband absorption until the anomalous Brewster effect (ABE) [40] was proposed very recently. The ABE establishes ultrabroadband impedance matching between free space and anisotropic absorptive materials, thus bestowing reflectionless absorption of light over a wide spectrum. Although microwave absorbers are demonstrated to verify the concept and principle of the ABE [40], a design strategy for metasurfaces exhibiting ultrabroadband reflectionless absorption operating at visible and near-infrared wavelengths is currently lacking.

In this work, we analyze and numerically demonstrate a type of nonresonant impedance-matched metasurface exhibiting ultrabroadband reflectionless absorption based on the ABE, which is denoted as an optical Brewster metasurface here. Compared with traditional resonant optical absorbers [9–15], the Brewster metasurface exhibits a remarkable property, i.e., ultrabroadband extreme angular asymmetry that varies from perfect transparency to perfect absorption. This effect is bestowed by the coexistence of the traditional BE and ABE, which occur correspondingly at incident angles with opposite signs, due to protection by the principle of reciprocity. As shown schematically in Fig. 1(a), when TM-polarized light is incident from the left side under the Brewster angle (i.e., $\theta_i = \theta_B = \arctan \sqrt{\varepsilon_d}$,

where θ_i , θ_B , and ε_d are, respectively, the incident angle, the Brewster angle, and the relative permittivity of the dielectric host), perfect transmission of light is achieved. On the other hand, when the incident light is flipped to the right side with $\theta_i = -\theta_B$, reflectionless light absorption is obtained instead. The angle $-\theta_B$ is denoted as the anomalous Brewster angle.

The proposed optical Brewster metasurface is composed of a periodic array of tilted metal films embedded in a dielectric host. The material-selection guidelines are systematically and quantitatively evaluated based on an effective-medium description for visible and near-infrared wavelengths. It is found that low-index dielectric materials like SiO_2 and MgF_2 are promising candidates for the dielectric host. On the other hand, metals possessing a permittivity with a small real part and a large imaginary part, like titanium (Ti), vanadium (V), chromium (Cr), molybdenum (Mo), and tungsten (W), are excellent candidates for the metal films. Numerical calculations show that near-perfect absorption can be obtained over the entire range of the visible spectrum and even extends into the infrared regime. Moreover, we demonstrate that ultrabroadband light absorption can be extended from the anomalous Brewster angle, $-\theta_B$, to the traditional Brewster angle, θ_B , by using a metal back-reflector or a folded metasurface, so that angular asymmetry is removed and the absorption performance is enhanced. Through engineering the tilt angle of metal films, a gradient optical Brewster metasurface exhibiting ultrabroadband and near-omnidirectional reflectionless absorption is demonstrated.

II. OPTICAL BREWSTER METASURFACES AND THE UNDERLYING PHYSICS

The schematic graph of the proposed optical Brewster metasurface is shown in Fig. 1(a). It is composed of a periodic array of tilted metal films (relative permittivity ε_m , thickness t , tilt angle α) aligned along the

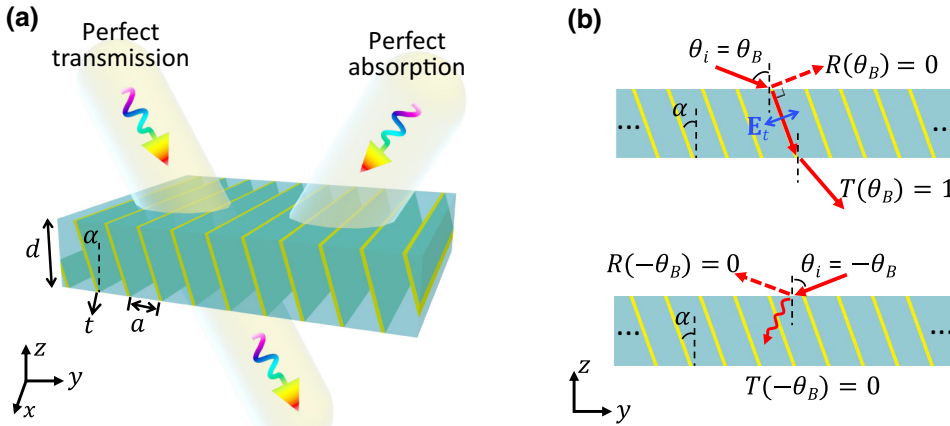


FIG. 1. (a) Schematic layout of an ultrabroadband reflectionless optical Brewster metasurface exhibiting extreme angular asymmetry. Metasurface consists of a periodic array of metal films embedded in a dielectric host. (b) Upper panel, ultrabroadband perfect transparency due to the BE under an incident angle of $\theta_i = \theta_B$. Lower panel, ultrabroadband perfect absorption due to the ABE under $\theta_i = -\theta_B$.

y direction in a dielectric host (relative permittivity ϵ_d , thickness d). The separation distance between two adjacent metal films is a , which is much larger than t (i.e., $a \gg t$), but smaller than free-space wavelength λ_0 to avoid diffraction.

We know that when TM-polarized light (magnetic field along the x direction) is incident onto the dielectric host in the absence of metal films, the reflection disappears under the Brewster angle $\theta_B = \arctan \sqrt{\epsilon_d}$ [38,39]. Generally, the chromatic dispersion of conventional dielectrics such as SiO_2 (about $-0.035 \mu\text{m}^{-1}$) and MgF_2 (about $-0.019 \mu\text{m}^{-1}$) is very weak in the optical regime [41], thus making it possible to obtain BE-induced zero reflection over the entire visible spectral range. In this case, the refracted light is normal to the direction of specular reflection, and the angle of refraction is $\theta_t = 90^\circ - \theta_B$. Interestingly, when ultrathin metal films are placed parallel to the direction of refracted light (i.e., $\alpha = \theta_t = 90^\circ - \theta_B$), the BE will not be destroyed, as illustrated in the upper panel of Fig. 1(b). This is because the refracted light cannot “see” such ultrathin metal films, as electric field \mathbf{E}_t is perpendicular to these metal films [42], and therefore, cannot be influenced by the metal films. As a result, the ultrabroadband zero reflection under the Brewster angle, θ_B , is preserved, even in the presence of metal films with $\alpha = 90^\circ - \theta_B$.

It becomes interesting when the reciprocity principle [43] is applied. Now, we consider flipping the incident

angle from θ_B to $-\theta_B$ [lower panel of Fig. 1(b)]. According to the reciprocity principle, the ultrabroadband zero reflection remains unchanged [43]. However, the electric field of refracted light is no longer perpendicular to the metal films. In this case, currents would be induced along the metal films, leading to the dissipation of refracted light. As a result, the ultrabroadband reflectionless absorption of light under $\theta_i = -\theta_B$, as strictly protected by the reciprocity principle, can be obtained. The angle $-\theta_B$ thus can be denoted as the anomalous Brewster angle, and the reflectionless phenomenon can be denoted as the ABE [40]. The optical metasurface exhibiting the ABE is denoted as the optical Brewster metasurface.

Therefore, when switching the incident angle from the traditional Brewster angle, θ_B , to the anomalous Brewster angle, $-\theta_B$, TM-polarized light will experience extreme angular asymmetry from perfect transparency to perfect absorption over an ultrawide spectrum. As a practical example, we take SiO_2 as the dielectric host, the refractive index of which is approximately considered to be a constant of 1.46 over the studied wavelength range of 400–1400 nm, and thus, the Brewster angle is fixed at $\theta_B = 55.6^\circ$. The metal films are made of Cr with $t = 10 \text{ nm}$, $a = 100 \text{ nm}$, and $d = 400 \text{ nm}$. These Cr films are ultrathin, satisfying the condition $t \ll a < \lambda_0$. The tilt angle is set as $\alpha = 90^\circ - \theta_B = 34.4^\circ$, such that there will be no reflection for light under $\theta_i = \pm\theta_B = \pm 55.6^\circ$ due to the BE and ABE.

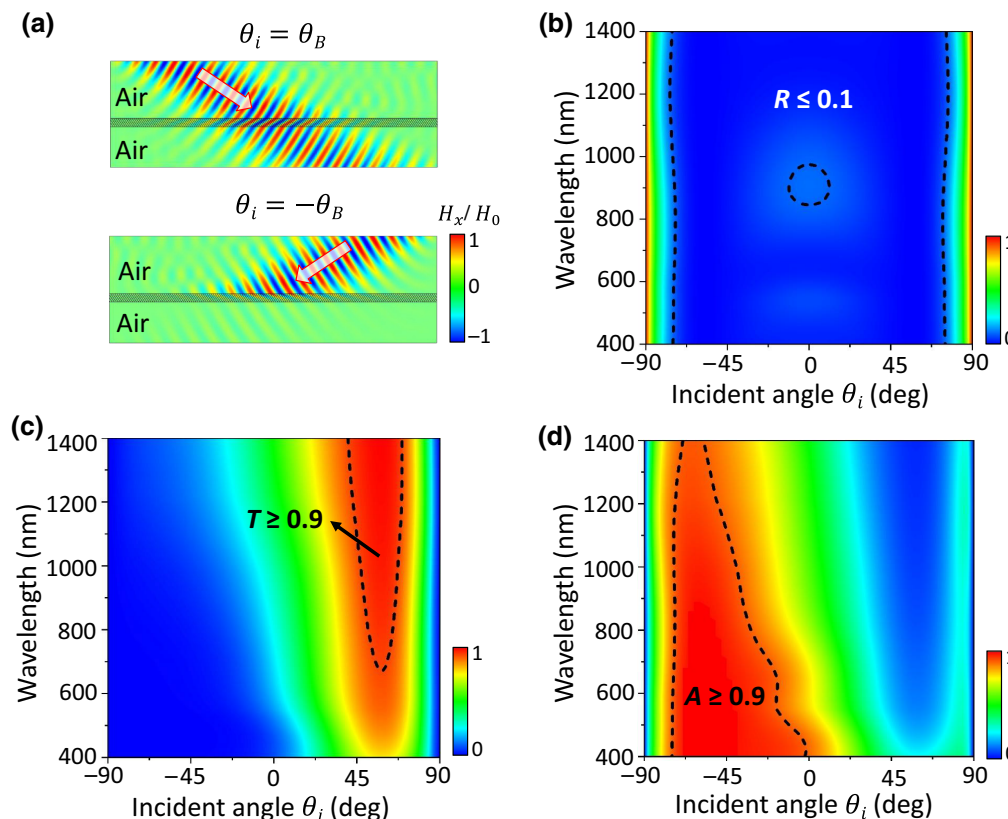


FIG. 2. (a) Simulated normalized magnetic field, H_x/H_0 , distributions under illumination of TM-polarized Gaussian beams with $\theta_i = \theta_B = 55.6^\circ$ (upper) and $\theta_i = -\theta_B = -55.6^\circ$ (lower) at $\lambda_0 = 800 \text{ nm}$. Brewster metasurface consists of tilted Cr films in a SiO_2 host. Relevant parameters are $a = 100 \text{ nm}$, $t = 10 \text{ nm}$, $d = 400 \text{ nm}$, and $\alpha = 34.4^\circ$. (b) Reflectance, (c) transmittance, and (d) absorptance as functions of the incident angle and working wavelength.

Direct numerical proof is presented in Fig. 2 using the software COMSOL Multiphysics. Here, we consider TM-polarized light, the magnetic field of which is polarized along the x direction with an amplitude of H_0 . Figure 2(a) shows the simulated normalized magnetic field, H_x/H_0 , distributions under the illumination of TM-polarized Gaussian beams with $\theta_i = \theta_B = 55.6^\circ$ (upper panel) and $\theta_i = -\theta_B = -55.6^\circ$ (lower panel) at $\lambda_0 = 800$ nm. Clearly, reflection is absent in both cases. Meanwhile, perfect transmission is observed under $\theta_i = \theta_B = 55.6^\circ$, in which case, light entering the metasurface propagates along the Cr films. While, under $\theta_i = -\theta_B = -55.6^\circ$, almost all incident light is absorbed. Moreover, we calculate reflectance R , transmittance T , and absorptance A as functions of the incident angle, θ_i , and working wavelength, as plotted in Figs. 2(b)–2(d), respectively. The dispersive parameter of Cr is taken from Ref. [41]. Here, the working wavelength is much larger than the separation distance, a , and therefore, diffraction is absent. We see that the reflection is symmetric with respect to θ_i and is quite low ($R < 0.1$) for all angles $|\theta_i| \leq 75^\circ$. In particular, under $\theta_i = \pm\theta_B = \pm 55.6^\circ$, we have $R < 0.01$ in the spectrum from 400 to 1400 nm. On the other hand, the transmission and absorption show a distinctly asymmetric behavior. Near-perfect transmission under $\theta_i = \theta_B = 55.6^\circ$ and near-perfect absorption under $\theta_i = -\theta_B = -55.6^\circ$ are observed over a wide spectrum. We note that the transmission and absorption vary with wavelength because of the finite thickness of the optical Brewster metasurface and the dispersion of Cr films.

Generally, for a fixed thickness, we have higher absorption and lower transmission for shorter wavelengths, as observed in Figs. 2(c) and 2(d).

It is noteworthy that the extreme angular asymmetry of the optical Brewster metasurface is robust against variations of the geometrical parameters. In Figs. 3(a) and 3(b), we successively change the separation distance, a , and thickness, t , of Cr films. The green, blue, and red lines denote, respectively, absorptance under $\theta_i = -\theta_B = -55.6^\circ$, transmittance under $\theta_i = \theta_B = 55.6^\circ$, and reflectance under $\theta_i = \pm\theta_B = \pm 55.6^\circ$ at $\lambda_0 = 800$ nm. We see that the near-zero reflection remains almost unchanged. High transmission due to the BE and near-perfect absorption due to the ABE are still seen. From Fig. 3(b), one may notice that the transmission decreases as t increases. This is because the refracted light can “see” the Cr films if they are not ultrathin. Moreover, we demonstrate an optical Brewster metasurface with random a and t in different transversal positions, as shown schematically in Fig. 3(c). Figure 3(d) presents the H_x/H_0 distribution when a TM-polarized Gaussian beam is incident onto the random metasurface under $\theta_i = \theta_B = 55.6^\circ$ (upper panel) and $\theta_i = -\theta_B = -55.6^\circ$ (lower panel), showing the occurrence of near-perfect transmission due to the BE and near-perfect absorption due to the ABE. These results manifest the robustness of the extreme angular asymmetry in the presence of imperfections of the Brewster metasurface, facilitating practical fabrication in experiments.

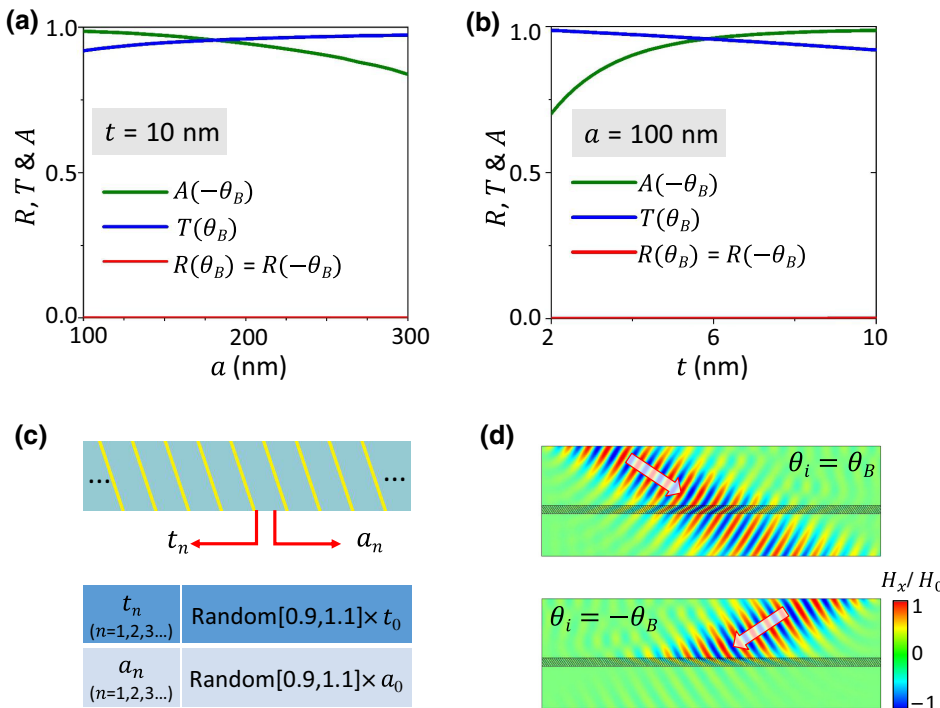


FIG. 3. Reflectance under $\theta_i = \pm\theta_B = \pm 55.6^\circ$, transmittance under $\theta_i = \theta_B = 55.6^\circ$, and absorptance under $\theta_i = -\theta_B = -55.6^\circ$ when (a) separation distance, a , is changed with fixed $t = 10$ nm, and (b) thickness of Cr films, t , is changed with fixed $a = 100$ nm. (c) Schematic graph of an optical Brewster metasurface with random a and t in different transversal positions. a varies randomly over the range from $0.9a_0$ to $1.1a_0$ with $a_0 = 100$ nm, and t varies randomly over the range from $0.9t_0$ to $1.1t_0$ with $t_0 = 10$ nm. (d) Simulated H_x/H_0 distributions when a TM-polarized Gaussian beam is incident from air onto the random metasurface under $\theta_i = \theta_B = 55.6^\circ$ (upper) and $\theta_i = -\theta_B = -55.6^\circ$ (lower). Working wavelength in (a)–(d) is 800 nm.

III. EFFECTIVE-MEDIUM DESCRIPTION AND EVALUATION OF MATERIAL SELECTION

The above results can also be understood from the perspective of an effective-medium model. For wavelengths much larger than the separation distance, a , the metasurface can be approximately homogenized as an effective anisotropic medium with $\varepsilon_{\perp} = (\varepsilon_m \varepsilon_d a \cos \alpha) / [\varepsilon_m(a \cos \alpha - t) + \varepsilon_d t]$ and $\varepsilon_{\parallel} = \varepsilon_d + (\varepsilon_m - \varepsilon_d) / [(a \cos \alpha)t]$, which are, respectively, the effective permittivities normal and parallel to the metal films [44,45]. Considering the limit of $t \ll a$, ε_{\perp} can be simplified to $\varepsilon_{\perp} \approx \varepsilon_d$. When light is incident under $\theta_i = \theta_B$, the electric field of refracted light is polarized along the direction of ε_{\perp} , which is irrelevant for the metal films. Therefore, for the incident light, the metal films do not seem to exist. Intriguingly, when flipping the incident angle to the anomalous Brewster angle, $-\theta_B$, zero reflection is preserved according to the reciprocity principle, but refracted light can “see” both ε_{\perp} and ε_{\parallel} .

Since ε_{\parallel} is ε_m dependent, incident light under $\theta_i = -\theta_B$ would be absorbed by metal films. Here, we express ε_m in a complex form as $\varepsilon_m = \varepsilon'_m + i\varepsilon''_m$, with ε'_m and ε''_m being the real and imaginary parts, respectively. Generally, the real part, ε'_m , has a negative value for Drude metals like silver and gold in the optical regime, and its absolute value becomes larger for longer wavelengths. However, a large absolute value of ε'_m would lead to a short skin depth for light in metals, hindering the absorption of light. On the other hand, the imaginary part, ε''_m , should be large; otherwise, the imaginary part of ε_{\parallel} would be negligibly small due to $t \ll a$. Therefore, to gain high-efficiency light absorption, the metal films should satisfy the condition $|\varepsilon''_m| \gg |\varepsilon'_m| \sim \varepsilon_d$ over a wide spectrum. This is the reason that the metal Cr, instead of silver or gold, is chosen here. The permittivity of Cr is found to

be $\varepsilon_m = -2.0 + 21.9i$ at 800 nm and approximately fulfills the condition $|\varepsilon''_m| \gg |\varepsilon'_m| \sim \varepsilon_d$ over the spectrum of 400–1400 nm [41]. Besides Cr, we find that V, W, Ti, and Mo are also promising candidate metals for optical Brewster metasurfaces. We note that a metasurface consisting of such highly dissipative metals usually does not support surface plasmons, and therefore, the geometrical interpretation presented in Fig. 1 is still valid here.

To demonstrate, we recalculate the absorptance of the metasurface in Fig. 2 under $\theta_i = -\theta_B = -55.6^\circ$, when different kinds of metal films are exploited instead, as plotted in Fig. 4(a). Evidently, high absorption is observed in the spectrum over 400–1400 nm. Since the reflection is absent due to the ABE, the absorptance can be further increased to be near unity through simply increasing the thickness, d , of the metasurface. Figure 4(b) presents the absorptance as a function of d at $\lambda_0 = 800$ nm, showing that near-perfect absorption of light can be obtained within a thickness of one wavelength.

To quantitatively evaluate the absorption efficiency, we express the magnetic field of light inside the metasurface as $H_0 e^{i(k_y y + k_z z) - i\omega t}$, where $k_x (= k_0 \sin \theta_i)$ and k_z are, respectively, the x and z components of the wave vector inside the metasurface. k_0 is the wave number in free space, and ω is the angular frequency. Due to material loss, k_z is a complex value, and thus, can be expressed as $k_z = k'_z + ik$, with k'_z and κ being the real and imaginary parts, respectively. This indicates that the refracted light decays exponentially at a rate of κ . Since there is no reflection, a larger decay rate indicates a higher absorption efficiency. k_x and k_z are connected by the dispersion of the effective medium as [46]

$$k_y^2 \varepsilon_{yy} + k_z^2 \varepsilon_{zz} + k_y k_z (\varepsilon_{yz} + \varepsilon_{zy}) = (\varepsilon_{yy} \varepsilon_{zz} - \varepsilon_{yz} \varepsilon_{zy}) k_0^2, \quad (1)$$

where ε_{yy} , ε_{yz} , ε_{zy} , and ε_{zz} are the terms of the permittivity tensor $\bar{\varepsilon} = \begin{pmatrix} \varepsilon_{yy} & \varepsilon_{yz} \\ \varepsilon_{zy} & \varepsilon_{zz} \end{pmatrix} = \begin{bmatrix} \varepsilon_{\perp} \cos^2 \alpha + \varepsilon_{\parallel} \sin^2 \alpha & (\varepsilon_{\perp} - \varepsilon_{\parallel}) \sin \alpha \cos \alpha \\ (\varepsilon_{\perp} - \varepsilon_{\parallel}) \sin \alpha \cos \alpha & \varepsilon_{\perp} \sin^2 \alpha + \varepsilon_{\parallel} \cos^2 \alpha \end{bmatrix}$. Considering the condition $|\varepsilon''_m| \gg |\varepsilon'_m| \sim \varepsilon_d$, ε_{\parallel} can be simplified to $\varepsilon_{\parallel} \approx \varepsilon_d + i\gamma$ with $\gamma = \varepsilon''_m / [(a \cos \alpha)t]$. Separating the real and imaginary parts of Eq. (1), and eliminating the variable k'_z , yields

$$\begin{aligned} \left(\frac{\kappa}{k_0}\right)^3 [\gamma^2 + (1 + \varepsilon_d)^2]^2 + 4 \left(\frac{\kappa}{k_0}\right)^2 \gamma \sqrt{1 + \varepsilon_d} [\gamma^2 + (1 + \varepsilon_d)^2] + \left(\frac{\kappa}{k_0}\right) (1 + \varepsilon_d) \\ \times [\gamma^4 + \varepsilon_d^2 (1 + \varepsilon_d)^2 + \gamma^2 (5 + 2\varepsilon_d + 2\varepsilon_d^2)] + 2\gamma (1 + \varepsilon_d)^{3/2} (\gamma^2 + \varepsilon_d^2) = 0. \end{aligned} \quad (2)$$

Based on Eq. (2), we plot the normalized decay rate, $|\kappa|/k_0$, with respect to ε''_m [the black solid line in Fig. 4(c)], showing a maximal decay rate occurring at $\varepsilon''_m = 23.92$.

The vertical dashed lines denote the values of ε''_m of V, W, Ti, Mo, and Cr. We find that all these values are close to the optimal value, i.e., $\varepsilon''_m = 23.92$. This further confirms

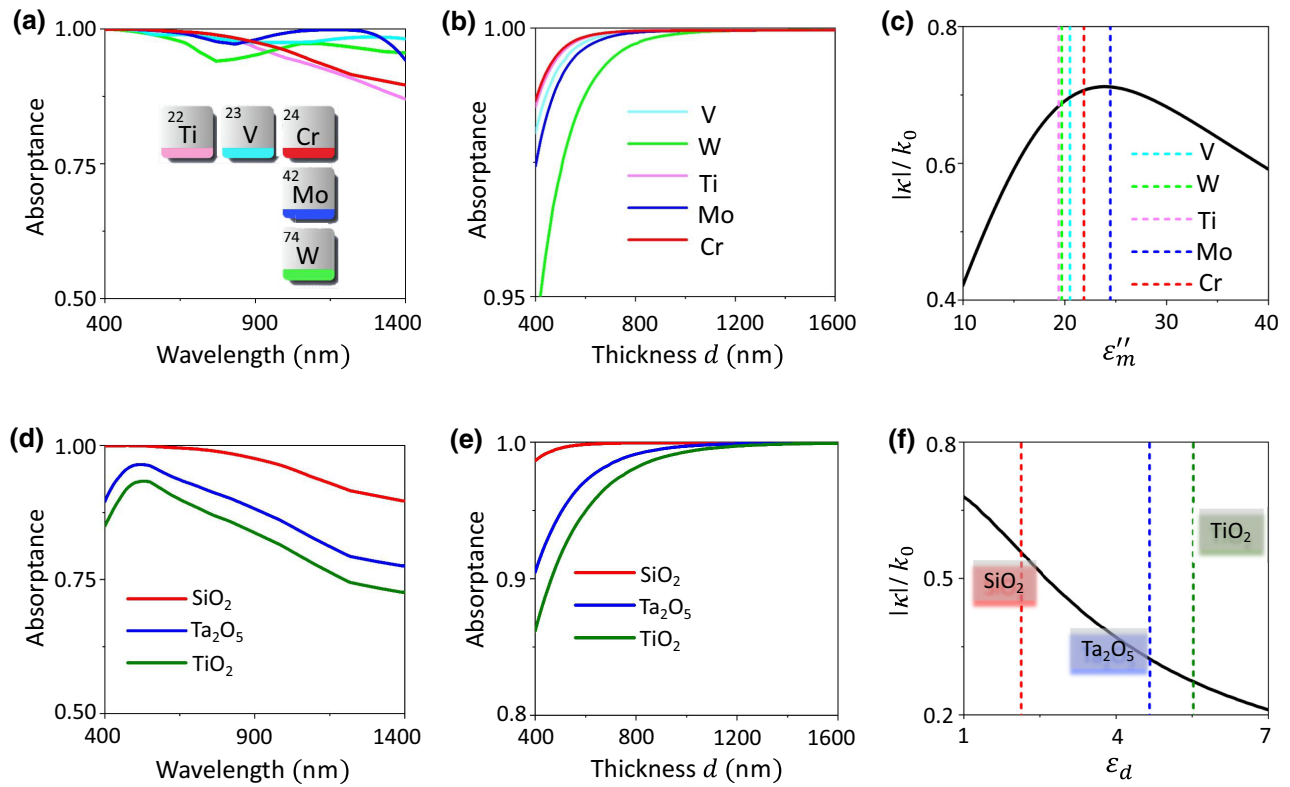


FIG. 4. (a) Absorption spectra under $\theta_i = -\theta_B = -55.6^\circ$. Metasurface is the same as that in Fig. 2 except for the metal-film materials. (b) Absorptance under $\theta_i = -\theta_B = -55.6^\circ$ at $\lambda_0 = 800$ nm when the thickness, d , is increased. (c) Normalized decay rate of light in the metasurface as a function of ϵ_m'' (black solid line). Vertical dashed lines denote values of ϵ_m'' of V, W, Ti, Mo, and Cr. (d) Absorption spectra under $\theta_i = -\theta_B$. Metasurface is the same as that in Fig. 2, except for the dielectric host materials. θ_B changes accordingly for different dielectric hosts. (e) Absorptance under $\theta_i = -\theta_B$ at $\lambda_0 = 800$ nm with increasing thickness d . (f) Normalized decay rate as a function of ϵ_d (black solid line). Vertical dashed lines denote values of ϵ_d of SiO_2 , Ta_2O_5 , and TiO_2 .

that V, W, Ti, Mo, and Cr are excellent candidate metals for high-efficiency optical Brewster metasurfaces.

Besides the metals, the dielectric hosts also affect the absorption efficiency, as both ϵ_\perp and ϵ_\parallel are ϵ_d dependent. To explore this influence, we use high-index tantalum pentoxide (Ta_2O_5) and titanium dioxide (TiO_2) for comparison, the refractive indices of which are 2.16 and 2.35, respectively. Figure 4(d) presents the absorption spectra of the metasurface in Fig. 2 under the anomalous Brewster angle, $\theta_i = -\theta_B = -\arctan \sqrt{\epsilon_d}$, when different kinds of dielectric hosts are considered. Since θ_B relies on ϵ_d , the incident angle is changed accordingly for different dielectric hosts. It is seen that the absorption decreases when the high-index host is utilized. Through increasing thickness d , near-perfect light absorption can still be obtained, as shown in Fig. 4(e). This indicates that the imperfection of absorption in Fig. 4(d) is attributed to the small decay rate, rather than the reflection. For further verification, we plot the normalized decay rate, $|\kappa|/k_0$, as a function of ϵ_d , as presented by the black solid line in Fig. 4(f). It is clearly seen that the decay rate decreases as ϵ_d increases. Since SiO_2 possesses the smallest refractive index among the

three dielectrics, the absorption efficiency is the highest, as observed in Fig. 4(d).

The material selection for the dielectric host affects not only the absorption efficiency, but also the absorption bandwidth. To gain ultrabroadband perfect absorption of light, the anomalous Brewster angle should be a constant value over an ultrawide spectrum, which requires a dispersionless ϵ_d . Within the spectrum of dispersionless ϵ_d , there is no extra restriction on the lower limit of the working frequency, while the upper limit is determined by the validity of the effective-medium approximation. Therefore, we can conclude that low-index dielectrics possessing low chromatic dispersions, like SiO_2 and MgF_2 , are promising candidate materials for ultrabroadband and high-efficiency optical Brewster metasurfaces.

IV. STRATEGIES TO IMPROVE ABSORPTION PERFORMANCE

In the following, we show that perfect absorption under the anomalous Brewster angle, $-\theta_B$, can be extended to the traditional Brewster angle, θ_B , so as to greatly improve

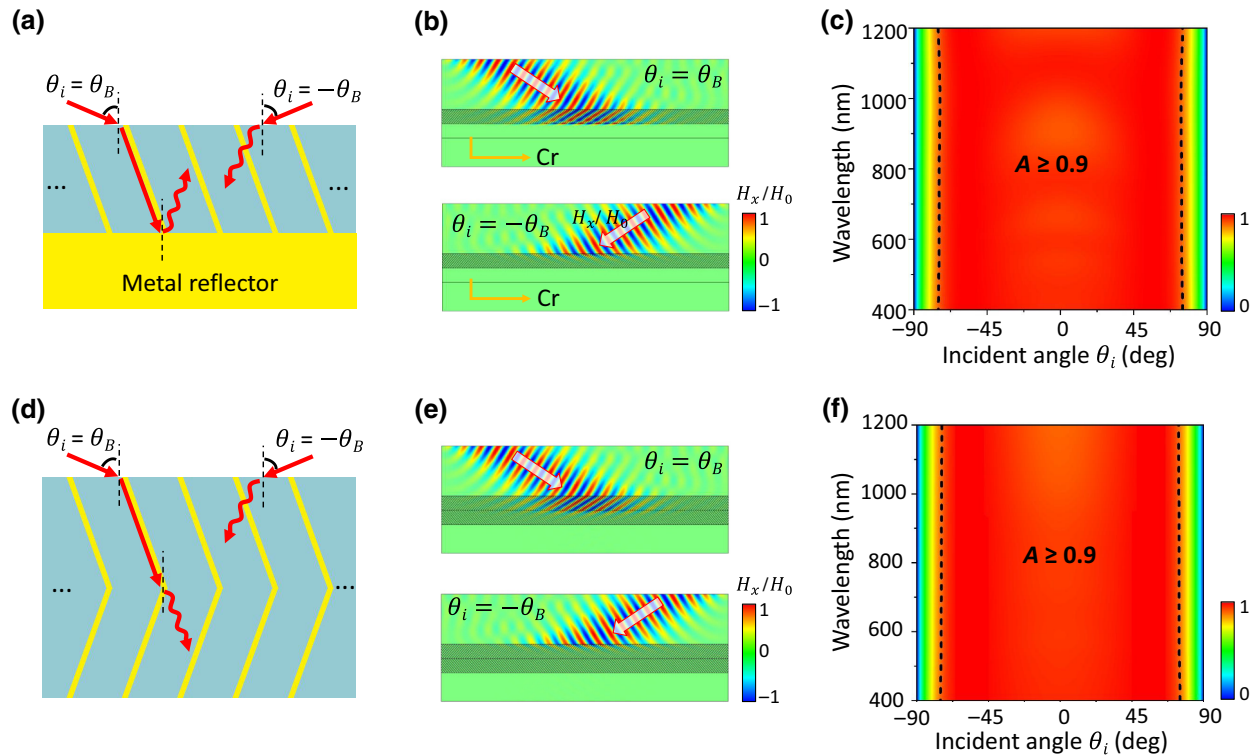


FIG. 5. Illustration of an optical Brewster metasurface with (a) metal back-reflector and (d) folded metasurface. (b),(e) Simulated H_x/H_0 distributions when a TM-polarized Gaussian beam is incident under $\theta_i = \theta_B = 55.6^\circ$ (upper) and $\theta_i = -\theta_B = -55.6^\circ$ (lower) at $\lambda_0 = 800$ nm. Relevant parameters are $a = 100$ nm, $t = 10$ nm, $d = 800$ nm, and $\alpha = 34.4^\circ$. In (b), the back-reflector is made of Cr. In (e), the bottom half is a folded metasurface. (c),(f) Absorptance as functions of the incident angle and working wavelength with regard to the metasurfaces in (b),(e), respectively.

the absorption performance. The first approach is to integrate a metal back-reflector. As illustrated in Fig. 5(a), under an incident angle of $\theta_i = \theta_B$, light can perfectly transmit into the metasurface because of the BE. Due to the back-reflector, the transmitted light will be reflected and then completely absorbed by the metal films. We note that there is no restriction on the choice of metals for the back-reflector. For simplicity, we utilize a bottom Cr layer to serve as the back-reflector. Figure 5(b) presents the simulated results for TM-polarized light under $\theta_i = \theta_B = 55.6^\circ$ (upper panel) and $\theta_i = -\theta_B = -55.6^\circ$ (lower panel) at $\lambda_0 = 800$ nm, showing near-perfect light absorption in both cases. Relevant parameters are $a = 100$ nm, $t = 10$ nm, $d = 800$ nm, and $\alpha = 34.4^\circ$. Moreover, the absorptance as functions of incident angle θ_i and the working wavelength is calculated and plotted in Fig. 5(c). We see that the absorption becomes symmetric with respect to θ_i and is significantly improved. High absorption ($A > 0.9$) is obtained for all angles $|\theta_i| \leq 75^\circ$ in the spectrum from 400 to 1400 nm.

The second approach is to integrate a folded Brewster metasurface. As illustrated in Fig. 5(d), the top half is

the same as that in Fig. 5(a), while the bottom half is a folded metasurface in which the tilt angle of metal films is flipped to $-\alpha$. In such a configuration, the incident light under $\theta_i = \theta_B$ can totally transmit through the top half and then be dissipated in the bottom half. For verification, we simulate the H_x/H_0 distributions for TM-polarized Gaussian beams with $\theta_i = \pm\theta_B = \pm 55.6^\circ$ at $\lambda_0 = 800$ nm [Fig. 5(e)]. As expected, all incident light is absorbed in both cases. In addition, the absorptance with respect to θ_i and working wavelength [Fig. 5(f)] indicates that the absorption performance of the metasurface is indeed greatly improved.

We note that the angle range of high absorption can be further enlarged by exploiting a high-index dielectric host, in which both the traditional and anomalous Brewster angles become larger. However, this would lead to a decrease of absorption efficiency, as discussed in Figs. 4(d)–4(f), indicating that a larger thickness of the metasurface is required to absorb the same amount of incident energy. Therefore, there is a trade-off between the angle range and absorption efficiency (or thickness) in the improvement of absorption performance.

V. GRADIENT OPTICAL BREWSTER METASURFACES FOR ULTRABROADBAND AND NEAR-OMNIDIRECTIONAL ABSORPTION

The above discussions suggest that, through harnessing the tilt angle of metal films inside the Brewster metasurface, reflectionless absorption over an ultrawide spectrum can be realized under a particular incident angle, i.e., the anomalous Brewster angle, for light incident from free space. In the following, we would like to show that this extraordinary absorption can be extended to all incident angles when the light source and metasurface are in the same dielectric host.

As shown schematically in Fig. 6(a), we consider a point source and a gradient metasurface in the same dielectric host. First, we assume that each metal film is aligned along the direction of emitted light from the point source, satisfying the condition $\alpha = \theta_i$ everywhere (upper panel). In this case, all emitted light can transmit through the gradient metasurface without any reflection, similar to the traditional BE. Then, we flip the rotation angle from α to $-\alpha$ of each metal film; thus, a gradient metasurface satisfying the condition $\alpha = -\theta_i$ everywhere is constructed (lower panel). Considering the principle of reciprocity, there will be no reflection, like the ABE, while light entering the metasurface would be dissipated on the metal films, bestowing omnidirectional reflectionless absorption.

The numerical verification is performed through examining the radiation of a vertical electric dipole source (dipole moment 1 A m) between two Brewster metasurfaces in the SiO_2 host [Figs. 6(b) and 6(c)].

Both metasurfaces consist of ultrathin Cr films with $a = 100$ nm, $t = 10$ nm, and $d = 800$ nm. The rotation angle satisfies the condition $\alpha = \theta_i$ ($\alpha = -\theta_i$) everywhere in the upper (lower) metasurface. Figures 6(b) and 6(c) show the simulated magnetic field distributions at $\lambda_0 = 800$ nm and $\lambda_0 = 400$ nm, respectively. The well-defined dipole radiation patterns without clear interference patterns induced by reflection indicate the near-omnidirectional zero reflection on both metasurfaces. Meanwhile, the magnetic field is almost unchanged above the upper metasurface, but quite weak below the lower metasurface. These results clearly demonstrate the phenomenon of ultrabroadband and near-omnidirectional reflectionless transmission (or absorption) of light in gradient Brewster metasurfaces through simply engineering the tilt angle of metal films. In principle, this approach is applicable for the reflectionless manipulation of light of an arbitrary wavefront.

VI. DISCUSSION AND CONCLUSION

The hallmark advantage of the proposed optical Brewster metasurface is that the reflectionless characteristic is mostly determined by the dielectric host and is independent of the metal films. Due to the low chromatic dispersion of dielectric permittivity, the bandwidth of reflectionless absorption, in principle, can cover an ultrabroad spectrum, far beyond those of other absorber techniques. For example, tilted hyperbolic metamaterials using metal-dielectric multilayer composites are proposed to realize perfect light absorption [34,47–49]. Nevertheless, the absorption bandwidth is limited by strong dispersion of their metal components in the visible spectral

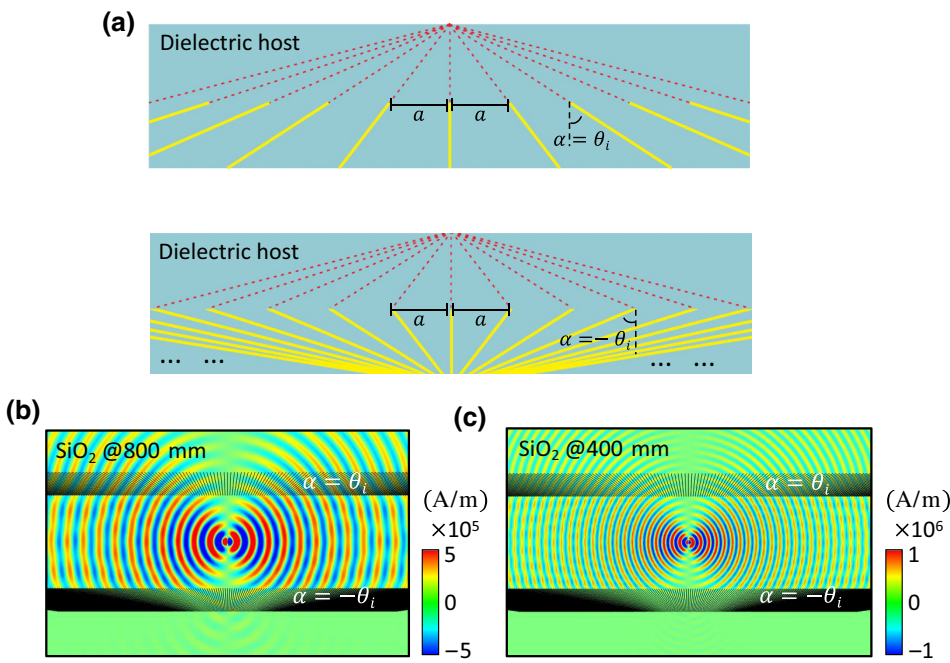


FIG. 6. (a) Schematic graphs of gradient metasurfaces with varied tilt angles of metal films satisfying $\alpha = \theta_i$ (upper) or $\alpha = -\theta_i$ (lower) everywhere in a dielectric host. Simulated magnetic field distributions when an electric dipole source is placed between two metasurfaces in the SiO_2 host at (b) $\lambda_0 = 800$ nm and (c) $\lambda_0 = 400$ nm. Upper (lower) metasurface satisfies the condition $\alpha = \theta_i$ ($\alpha = -\theta_i$) everywhere.

range, and thus, is inherently narrow. In addition, the absorption bandwidth of the optical Brewster metasurface can be further broadened through simply increasing its thickness.

The extreme angular asymmetry is another intriguing property of the optical Brewster metasurface. This phenomenon originates from the coexistence of the traditional BE and ABE occurring at the corresponding incident angles with opposite signs, and this is strictly protected by the reciprocity principle. Compared with schemes based on resonant metasurfaces and metagratings [35–37], our scheme has the advantages of simplicity, high efficiency, robustness, and ultrabroad bandwidth.

Practical implementation of the optical Brewster metasurface usually requires a dielectric substrate. Our numerical calculations reveal that the dielectric substrate generally will not affect the near-zero reflection under the traditional and anomalous Brewster angles, but will slightly reduce the transmission and increase the absorption under the traditional Brewster angle. This is because part of the incident light is reflected at the metasurface-substrate interface due to impedance mismatching and is then absorbed by the metasurface, similar to the situation in Fig. 5(a). One approach to mitigate impedance mismatching is to add an antireflection layer between the metasurface and substrate, which can eliminate reflection under a chosen incident angle. An alternative approach is to use an all-dielectric unidirectional complementary medium consisting of symmetric dielectric multilayers that can optically cancel out the substrate [50].

The principle of the optical Brewster metasurface is universal. Besides microwave, visible, and near-infrared frequencies, it can be easily extended to far-infrared and terahertz regimes, where ultrathin graphene might be an excellent candidate material. Due to the tunability of graphene [51,52], dynamically controllable ABE and absorption could become possible.

In summary, we demonstrate a simple but highly efficient approach to realize ultrabroadband reflectionless optical Brewster metasurfaces. Near-perfect absorption of light can be obtained over the entire visible spectral range and the near-infrared regime. The optical Brewster metasurfaces exhibit extreme angular asymmetry, based on which a transition from perfect transparency to perfect absorption is achieved due to the coexistence of the traditional BE and ABE occurring at incident angles with opposite signs. We systematically and quantitatively evaluate the material-selection guidelines for high-efficiency absorption. Strategies like the utilization of a metal back-reflector or a folded metasurface are proposed to remove the angular asymmetry in absorption and significantly improve the performance. A gradient optical Brewster metasurface exhibiting ultrabroadband and near-omnidirectional reflectionless absorption is also shown. Our findings offer a path towards high-efficiency light

absorption with ultrabroad bandwidth and extreme angular asymmetry.

ACKNOWLEDGMENTS

The authors acknowledge funding from the National Key R&D Program of China (Grants No. 2020YFA02 11300 and No. 2017YFA0303702), the National Natural Science Foundation of China (Grants No. 11974176 and No. 12174188), the Research Grants Council of Hong Kong (Grant No. R6015-18), and the Priority Academic Program Development of Jiangsu Higher Education Institutions (PAPD).

- [1] M. Long, P. Wang, H. Fang, and W. Hu, Progress, challenges, and opportunities for 2D material based photodetectors, *Adv. Funct. Mater.* **29**, 1803807 (2019).
- [2] D. G. Baranov, Y. Xiao, I. A. Nechepurenko, A. Krasnok, A. Alu, and M. A. Kats, Nanophotonic engineering of far-field thermal emitters, *Nat. Mater.* **18**, 920 (2019).
- [3] A. Polman, M. Knight, E. C. Garnett, B. Ehrler, and W. C. Sinke, Photovoltaic materials: Present efficiencies and future challenges, *Science* **352**, 307 (2016).
- [4] H. K. Raut, V. A. Ganesh, A. S. Nair, and S. Ramakrishna, Anti-reflective coatings: A critical, in-depth review, *Energ. Environ. Sci.* **4**, 3779 (2011).
- [5] S. Chattopadhyay, Y. F. Huang, Y. J. Jen, A. Ganguly, K. H. Chen, and L. C. Chen, Anti-reflecting and photonic nanostructures, *Mat. Sci. Eng. R* **69**, 1 (2010).
- [6] Y. Li, J. Zhang, and B. Yang, Antireflective surfaces based on biomimetic nanopillared arrays, *Nano Today* **5**, 117 (2010).
- [7] W. Dallenbach and W. Kleinsteuber, Reflection and absorption of decimeter-waves by plane dielectric layers, *Hochfreq. U Elektroak* **51**, 152 (1938).
- [8] W. W. Salisbury, Absorbent body of electromagnetic waves, U.S. Patent No. 2,599,944 (10 June 1952).
- [9] H. T. Chen, J. F. O'Hara, A. K. Azad, and A. J. Taylor, Manipulation of terahertz radiation using metamaterials, *Laser Photonics Rev.* **5**, 513 (2011).
- [10] C. M. Watts, X. Liu, and W. J. Padilla, Metamaterial electromagnetic wave absorbers, *Adv. Mater.* **24**, OP98 (2012).
- [11] Y. Cui, Y. He, Y. Jin, F. Ding, L. Yang, Y. Ye, S. Zhong, Y. Lin, and S. He, Plasmonic and metamaterial structures as electromagnetic absorbers, *Laser Photonics Rev.* **8**, 495 (2014).
- [12] Y. Ra'Di, C. R. Simovski, and S. A. Tretyakov, Thin Perfect Absorbers for Electromagnetic Waves: Theory, Design, and Realizations, *Phys. Rev. Appl.* **3**, 037001 (2015).
- [13] M. A. Kats and F. Capasso, Optical absorbers based on strong interference in ultra-thin films, *Laser Photonics Rev.* **10**, 735 (2016).
- [14] L. Feng, P. Huo, Y. Liang, and T. Xu, Photonic metamaterial absorbers: Morphology engineering and interdisciplinary applications, *Adv. Mater.* **2019**, 1903787 (2019).
- [15] Y. P. Lee, J. Y. Rhee, Y. J. Yoo, and K. W. Kim, *Metamaterials for Perfect Absorption* (Springer, Singapore, 2016).

- [16] J. Hao, J. Wang, X. Liu, W. J. Padilla, L. Zhou, and M. Qiu, High Performance Optical Absorber Based on a Plasmonic Metamaterial, *Appl. Phys. Lett.* **96**, 251104 (2010).
- [17] S. Thongrattanasiri, F. H. L. Koppens, F. J., and García De Abajo, Complete Optical Absorption in Periodically Patterned Graphene, *Phys. Rev. Lett.* **108**, 047401 (2012).
- [18] H. Lin, B. C. P. Sturmberg, K. Lin, Y. Yang, X. Zheng, T. K. Chong, C. M. de Sterke, and B. Jia, A 90-nm-thick graphene metamaterial for strong and extremely broadband absorption of unpolarized light, *Nat. Photonics* **13**, 270 (2019).
- [19] Q. Feng, M. Pu, C. Hu, and X. Luo, Engineering the dispersion of metamaterial surface for broadband infrared absorption, *Opt. Lett.* **37**, 2133 (2012).
- [20] D. Ye, Z. Wang, K. Xu, H. Li, J. Huangfu, Z. Wang, and L. Ran, Ultrawideband Dispersion Control of a Metamaterial Surface for Perfectly-Matched-Layer-Like Absorption, *Phys. Rev. Lett.* **111**, 187402 (2013).
- [21] G. James, M. Yong, S. Shimul, K. Ata, and D. R. S. Cumming, Polarization insensitive, broadband terahertz metamaterial absorber, *Opt. Lett.* **36**, 3476 (2011).
- [22] J. Sun, L. Liu, G. Dong, and J. Zhou, An extremely broad band metamaterial absorber based on destructive interference, *Opt. Express* **19**, 21155 (2011).
- [23] X. Shen, T. J. Cui, J. Zhao, H. F. Ma, W. X. Jiang, and H. Li, Polarization-independent wide-angle triple-band metamaterial absorber, *Opt. Express* **19**, 9401 (2011).
- [24] Y. Cui, K. H. Fung, J. Xu, H. Ma, Y. Jin, S. He, and N. X. Fang, Ultrabroadband light absorption by a sawtooth anisotropic metamaterial slab, *Nano Lett.* **12**, 1443 (2012).
- [25] Y. Z. Cheng, W. Withayachumnankul, A. Upadhyay, D. Headland, Y. Nie, R. Z. Gong, M. Bhaskaran, S. Sriram, and D. Abbott, Ultrabroadband plasmonic absorber for terahertz waves, *Adv. Opt. Mater.* **3**, 376 (2015).
- [26] F. Ding, Y. Jin, B. Li, H. Cheng, L. Mo, and S. He, Ultrabroadband strong light absorption based on thin multi-layered metamaterials, *Laser Photonics Rev.* **8**, 946 (2014).
- [27] C. Yang, C. Ji, W. Shen, K. Lee, Y. Zhang, X. Liu, and L. J. Guo, Compact multilayer film structures for ultra-broadband, omnidirectional, and efficient absorption, *ACS Photonics* **3**, 590 (2016).
- [28] M. Yang, S. Chen, C. Fu, and P. Sheng, Optimal sound-absorbing structures, *Mater. Horiz.* **4**, 673 (2017).
- [29] S. Wu, Y. Ye, Z. Jiang, T. Yang, and L. Chen, Large-area, ultrathin metasurface exhibiting strong unpolarized ultrabroadband absorption, *Adv. Opt. Mater.* **7**, 1901162 (2019).
- [30] L. Zhou, Y. Tan, J. Wang, W. Xu, Y. Yuan, W. Cai, S. Zhu, and J. Zhu, 3D self-assembly of aluminium nanoparticles for plasmon-enhanced solar desalination, *Nat. Photonics* **10**, 393 (2016).
- [31] L. Zhou, Y. Tan, D. Ji, B. Zhu, P. Zhang, J. Xu, Q. Gan, Z. Yu, and J. Zhu, Self-assembly of highly efficient, broadband plasmonic absorbers for solar steam generation, *Sci. Adv.* **2**, e1501227 (2016).
- [32] H. Zhang, L. Feng, Y. Liang, and T. Xu, An ultra-flexible plasmonic metamaterial film for efficient omnidirectional and broadband optical absorption, *Nanoscale* **11**, 437 (2019).
- [33] J. U. Kim, S. Lee, S. J. Kang, and T. Kim, Materials and design of nanostructured broadband light absorbers for advanced light-to-heat conversion, *Nanoscale* **10**, 21555 (2018).
- [34] X. Wu, C. A. McEleney, M. González-Jiménez, and R. Macêdo, Emergent asymmetries and enhancement in the absorption of natural hyperbolic crystals, *Optica* **6**, 1478 (2019).
- [35] X. Wang, A. Diaz-Rubio, V. S. Asadchy, G. Ptitsyn, A. A. Generalov, J. Ala-Laurinaho, and S. A. Tretyakov, Extreme Asymmetry in Metasurfaces via Evanescent Fields Engineering: Angular-Asymmetric Absorption, *Phys. Rev. Lett.* **121**, 256802 (2018).
- [36] Y. Cao, Y. Fu, Q. Zhou, X. Ou, L. Gao, H. Chen, and Y. Xu, Mechanism Behind Angularly Asymmetric Diffraction in Phase-Gradient Metasurfaces, *Phys. Rev. Appl.* **12**, 024006 (2019).
- [37] S. Dong, G. Hu, Q. Wang, Y. Jia, Q. Zhang, G. Cao, J. Wang, S. Chen, D. Fan, W. Jiang, Y. Li, A. Alù, and C. Qiu, Loss-assisted metasurface at an exceptional point, *ACS Photonics* **7**, 3321 (2020).
- [38] D. Brewster, On the laws which regulate the polarisation of light by reflexion from transparent bodies, *Philos. Trans. R. Soc.* **105**, 125 (1815).
- [39] A. Lakhtakia, Would brewster recognize today's brewster angle?, *Optics News* **15**, 14 (1989).
- [40] J. Luo, H. Chu, R. Peng, M. Wang, J. Li, and Y. Lai, Ultra-broadband reflectionless brewster absorber protected by reciprocity, *Light-Sci. Appl.* **10**, 89 (2021).
- [41] RefractiveIndex.INFO, <http://refractiveindex.info/>.
- [42] J. B. Pendry, A. J. Holden, D. J. Robbins, and W. J. Stewart, Low frequency plasmons in thin-wire structures, *J. Phys.-Condens. Mat.* **10**, 4785 (1998).
- [43] R. J. Potton, Reciprocity in optics, *Rep. Prog. Phys.* **67**, 717 (2004).
- [44] V. A. Markel, Introduction to the Maxwell garnett approximation: Tutorial, *J. Opt. Soc. Am. A* **33**, 1244 (2016).
- [45] T. Dong, J. Luo, H. Chu, X. Xiong, R. Peng, M. Wang, and Y. Lai, Breakdown of Maxwell garnett theory due to evanescent fields at deep-subwavelength scale, *Photonics Res.* **9**, 848 (2021).
- [46] S. Shah, Y. Jiang, L. Song, H. Wang, and L. Shen, Optical axis-driven field discontinuity in a hyperbolic medium, *Opt. Lett.* **45**, 3067 (2020).
- [47] S. M. Hashemi and I. S. Nefedov, Wideband perfect absorption in arrays of tilted carbon nanotubes, *Phys. Rev. B* **86**, 195411 (2012).
- [48] I. S. Nefedov, C. A. Valagiannopoulos, S. M. Hashemi, and E. I. Nefedov, Total absorption in asymmetric hyperbolic media, *Sci. Rep.* **3**, 2662 (2013).
- [49] X. Wu and C. Fu, Manipulation of enhanced absorption with tilted hexagonal boron nitride slabs, *J. Quant. Spectrosc. Ra.* **209**, 150 (2018).
- [50] M. Huang, X. Li, and J. Luo, All-dielectric unidirectional complementary media for transmission enhancement, *Opt. Express* **28**, 33263 (2020).
- [51] A. Andryieuski and A. V. Lavrinenko, Graphene metamaterials based tunable terahertz absorber: Effective surface conductivity approach, *Opt. Express* **21**, 9144 (2013).
- [52] P. C. Wu, N. Papasimakis, and D. P. Tsai, Self-affine Graphene Metasurfaces for Tunable Broadband Absorption, *Phys. Rev. Appl.* **6**, 044019 (2016).